

Paint Deposition Modeling for Trajectory Planning on Automotive Surfaces

David C. Conner, *Student Member, IEEE*, Aaron Greenfield, *Student Member, IEEE*, Prasad N. Atkar, *Student Member, IEEE*, Alfred A. Rizzi, *Member, IEEE*, and Howie Choset, *Member, IEEE*

Abstract—This research is focused on developing trajectory planning tools for the automotive painting industry. The geometric complexity of automotive surfaces and the complexity of the spray patterns produced by modern paint atomizers combine to make this a challenging and interesting problem. This paper documents our efforts to develop computationally tractable analytic deposition models for electrostatic rotating bell (ESRB) atomizers, which have recently become widely used in the automotive painting industry. The models presented in this paper account for both the effects of surface curvature as well as the deposition pattern of ESRB atomizers in a computationally tractable form, enabling the development of automated trajectory generation tools. We present experimental results used to develop and validate the models, and verify the interaction between the deposition pattern, the atomizer trajectory, and the surface curvature. Limitations of the deposition model with respect to predictions of paint deposition on highly curved surfaces are discussed.

Note to Practitioners—The empirical paint deposition models developed herein, which are fit to experimental data, offer a significant improvement over models that are typically used in industrial robot simulations. The improved simulation results come without the computational cost and complexity of finite element methods. The models could be incorporated, as is, into existing industrial simulation tools, provided the users are cognizant of the model limitations with respect to highly curved surfaces. Although the models are based on readily available information, incorporating the models into existing robot simulation software would likely require support from the software vendor.

Index Terms—Automotive painting, trajectory planning, coverage.

I. INTRODUCTION

AUTOMATION is widely used for automotive paint application because of the repeatability of the resulting surface finish, as well as the benefit of removing humans from a hazardous environment. The automation of paint application became necessary with the advent of high speed rotating bell atomizers and electrostatic charging, both of which significantly increase transfer efficiency—the ratio of paint deposited on the target surface to the total paint used.

Manuscript received October 11, 2004. This paper was recommended for publication by Associate Editor S. Gupta and Editor M. Wang upon evaluation of the reviewers' comments. This work was supported by the National Science Foundation and the Ford Motor Company under Grant IIS-9987972.

D. C. Conner, A. Greenfield, A. A. Rizzi, and H. Choset are with the Robotics Institute, Carnegie Mellon University, Pittsburgh, PA 15213 USA (e-mail: dconner@cmu.edu; algaei@cs.cmu.edu; arizzi@cs.cmu.edu; choset@cmu.edu).

P. N. Atkar is with the Department of Mechanical Engineering, Carnegie Mellon University, Pittsburgh, PA 15213 USA (e-mail: atkar@cmu.edu).

Digital Object Identifier 10.1109/TASE.2005.851631

Increasingly, these atomizers are positioned by robot manipulators instead of fixed automation, as robot manipulators afford a greater level of system flexibility, allowing facilities to rapidly adapt to changes in automobile designs. While the task of applying paint has become almost completely automated, generating trajectories for the robots is largely a human endeavor based on the experience of skilled technicians. Automatic generation of trajectories can reduce the time required to deploy a paint system for a new vehicle, thus reducing the concept-to-customer time-line, and allows for a thorough evaluation of the trajectories against a set of performance criteria—including paint uniformity, paint waste, cycle time, etc. Unfortunately, the relatively complex deposition patterns produced by electrostatic rotating bell (ESRB) atomizers have made previous work in trajectory planning for deposition tasks inadequate.

The deposition model we present has two primary purposes: 1) to capture the structure of the deposition pattern for use in a planning system and 2) to support simulations used to evaluate potential planning methods. These two purposes lead to contradictory criteria for evaluating the models. First, the model must be accurate enough to capture the structure of the deposition and accurately predict the deposition on a variety of surface shapes used to validate planning methods. Existing deposition models designed for use in trajectory planning are too simple to capture the relevant effects. Second, the model must be computationally tractable from the perspective of the simulation and planning tools, since the model will be used within a planning system.

We have developed a family of deposition models that capture the significant features of the paint deposition process, while retaining an analytic representation. While the model is not intended to capture the full effects of the electrostatic field on curved surfaces, the model has proved useful in developing planning methods because it captures important features of the effect of surface curvature. Note that our planning methods, discussed in [1], [2], have been specifically developed to be independent of the deposition model.

Section II covers relevant prior work in paint deposition modeling. In Section III, we develop analytic paint deposition models. Although general, the models are specifically designed to capture the structure of the deposition pattern generated by high speed rotating bell atomizers widely used for automotive painting. We develop an analytic relation between the structure of the deposition pattern and the variability of the paint thickness on extruded surfaces. In Section IV, we discuss experimental tests and methods used to determine values for the parameters of the analytic deposition model. Further results of experiments, which were designed to validate the param-

eterized deposition model developed in Section III, are also presented. Finally, in Section V, we draw conclusions from the results and discuss the future direction of our work.

II. PRIOR WORK

The work presented in this paper is an outgrowth of our prior work in the area of coverage planning; we developed plans for guaranteeing complete coverage of previously unexplored and unknown planar regions [3], [4]. We later extended these ideas to reliably cover surfaces embedded in \mathbb{R}^3 [5]. While these prior efforts provided techniques for ensuring complete coverage of a surface, they did not address the problem of minimizing variation in coating thickness, which we term the *uniform coverage problem*.

Typical industrial robot planning/programming systems, such as RobCADTM Paint,¹ rely on the user to specify the paint distribution pattern in the form of a paint thickness profile curve. Since these tools do not consider the curvature of the surface being painted, the utility of these tools for reliable paint deposition simulation remains limited.

Most academic research into automated trajectory planning for painting robots assumed simple deposition models. The “automatic trajectory planning system” (ATPS) assumed uniform paint distribution in a circular pattern [6]. The “teachless” spray painting system, developed by Asakawa and Takeuchi [7], required a user specified set of parameters such as the elliptical diameters of the paint pattern and the desired distance between consecutive passes, which is known as the *index distance*. Sheng *et al.* [8] used a simple parabolic thickness profile with a circular deposition pattern. Freund *et al.* [9] proposed a simple bivariate Gaussian model for the paint deposition, and focused on calculation of the optimum index distance over planar sheets. Ramabhadran and Antonio [10] considered bivariate Cauchy or Gaussian distributions for the paint deposition applied to a flat panel.

Other simple models include Arikan and Balkan’s [11] paint deposition simulation model, which used a beta distribution. They considered the effect of the distribution pattern on the optimal index distance, along with a preliminary attempt at considering surface effects on the deposition. Hertling *et al.* [12], [13] focused on the development of deposition models, which match a series of basis functions to experimental data assuming an overall elliptical pattern. They reported that the observed deposition patterns were not uniform, and did not exhibit a parabolic profile as reported by other researchers.

The highly simplified deposition models used in the vast majority of prior research into paint deposition planning were developed specifically for aerosol spray atomizers [12]. Automotive coating processes are moving increasingly toward the use of ESRB atomizers in order to increase transfer efficiencies [14]–[16]. In an ESRB atomizer, paint fluid is forced onto the inner surface of a high speed rotating bell, which is maintained at a voltage of 50–90 kV relative to the grounded surface being painted. Fig. 1 shows a schematic of a typical atomizer configuration. The paint flow breaks up at the edge of the bell, forming a cloud of droplets, as it is expelled radially due to centrifugal

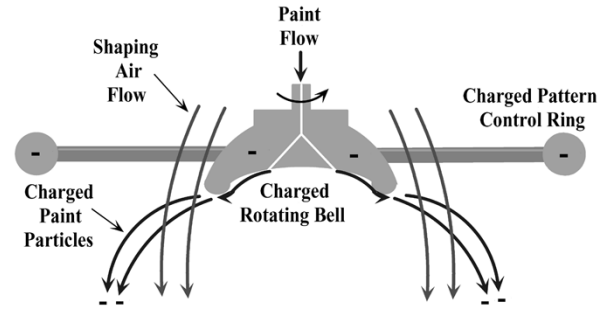


Fig. 1. ESRB atomizer with paint particle trajectory and shaping air flow lines shown.

force imparted to the paint by the rotating bell. Each resulting paint droplet is charged due to the charge on the bell. If the particle charge is above the Rayleigh limit, the droplet breaks apart under the resulting electrostatic forces, further atomizing the paint spray. Typical diameters for the paint droplets are in the range of 10–30 μm [14], [15]. High velocity shaping air, and often a charged pattern control ring, are used to direct the charged particles toward the target surface.

The combined aerodynamic and electrostatic effects on the paint spray and the resulting distribution of droplets on the target surface are complex. Limited modeling studies have been performed, and are generally based on finite element computational techniques [14]–[16]. The computational nature of these simulation approaches makes them unsuitable for direct use in a planning system, and have led us to investigate the use of empirically validated analytic models to capture the dominant structure of the deposition process.

III. DEPOSITION MODELING

The pattern of paint deposition, or film build, generated by ESRB atomizers is a function of the specific atomizer, process parameters, shape of the surface, and relative orientation of the atomizer to the surface. When the atomizer is stationary, we term the measured paint thickness over a surface as the two-dimensional (*2-D*) *deposition pattern*. As the atomizer passes over a surface, the majority of the paint emitted by the atomizer is deposited on the surface, although some paint is invariably entrained in the shaping air and lost. The total paint thickness at a given point on the surface depends on the rate of paint deposition, the path followed by the atomizer over the surface, and the speed at which the path is traversed [10]–[12]. We refer to the resulting cross section of paint thickness orthogonal to the direction of travel of the atomizer as the one-dimensional (*1-D*) *collapse*. Ideally, the 1-D collapse is equivalent to integration of the 2-D deposition model along the direction of travel. Fig. 2 shows the relationship between these structures for a planar surface.

A. 2-D Deposition Model

We have developed a 2-D deposition model that represents the rate of paint deposition or *deposition flux* in units of thickness per second at a given point on an arbitrary surface, given a specific path location and orientation of the atomizer. We denote our model by $D(\mathbf{s}, \mathbf{p}, \dot{\mathbf{p}})$, where $D : \{\mathbb{R}^3 \times \mathbf{S}^2\} \times SE(3) \times se(3) \rightarrow$

¹RobCAD is a trademark of Tecnomatix Technologies Ltd.

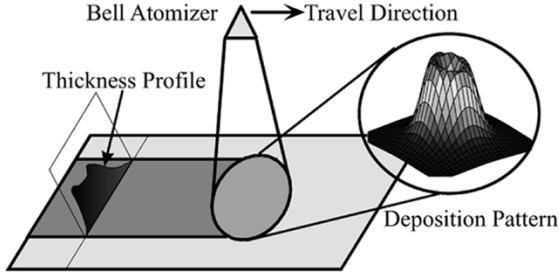


Fig. 2. Painting a flat panel shows the relationship between the 2-D deposition pattern and the integrated thickness profile (1-D collapse).

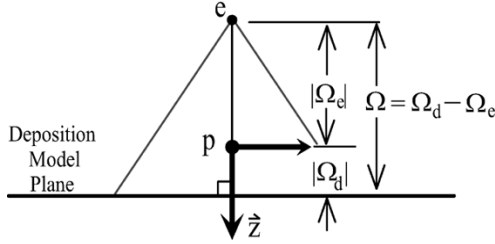


Fig. 3. Atomizer path location uniquely determines both the emission point and deposition model plane. As drawn, the signed value of Ω_e is negative since the emission point is behind the atomizer path location \mathbf{p} .

$[0, \infty)^2$, $\mathbf{s} \in \mathbb{R}^3 \times \mathbf{S}^2$ represents a point and the associated surface normal on the surface being painted, and $\mathbf{p} \in SE(3)$ represents a path location and orientation given by the tool center point frame (TCPF) specified by the planner and used by the robot control program. We refer to $D(\mathbf{s}, \mathbf{p}, \dot{\mathbf{p}})$ as the *2D deposition model*, or simply the *deposition model*.

Since parameterizing the deposition model for arbitrary surfaces is difficult at best, we choose to develop an analytic model by factoring the problem into three independent components. We begin by parameterizing the 2-D deposition pattern to give deposition flux on a planar surface. We refer to the analytic model for the planar surface as the *planar deposition model*. The planar surface is referred to as the *deposition model plane*, and is shown in Fig. 3. Next, through recourse to differential geometry, the planar deposition pattern is mapped onto an arbitrary surface in a manner that preserves the total paint volume. Finally, there is anecdotal evidence that the deposition rate also depends on atomizer velocity [17]. Thus, the total deposition flux model for a point on an arbitrary surface is a function of three sub-models: deposition on a plane, projection to the surface, and scaling by speed. Specifically, the total model is given by

$$D(\mathbf{s}, \mathbf{p}, \dot{\mathbf{p}}) = V_s(\dot{\mathbf{p}})AM(\mathbf{s}, \mathbf{p})d(\mathbf{q}(\mathbf{s}, \mathbf{p}))$$

where $d: \mathbb{R}^2 \rightarrow [0, \infty)$ is the deposition at a point on the deposition model plane determined by $\mathbf{q}: \mathbb{R}^3 \times SE(3) \rightarrow \mathbb{R}^2$, $AM: \{\mathbb{R}^3 \times \mathbf{S}^2\} \times SE(3) \rightarrow [0, \infty)$ is the area magnification factor of the projection, and $V_s: se(3) \rightarrow [0, \infty)$ is the speed scaling. We now detail each part.

1) *Planar Deposition Model*: We denote the planar deposition model as $d(\mathbf{q}) = d(x, y)$, where $d: \mathbb{R}^2 \rightarrow [0, \infty)$, and

\mathbf{S}^2 is the unit sphere, which is used to encode the surface normal of a 2-D surface embedded in \mathbb{R}^3 . $SE(3)$ is the *Special Euclidean Group*, which is used to encode position and orientation of rigid bodies in \mathbb{R}^3 . The corresponding Lie algebra, $se(3)$, is the tangent space at the identity of $SE(3)$.

$\mathbf{q} = (x, y)$ is a point on the deposition model plane determined by the projection model described in the next section. As shown in Fig. 3, the deposition model plane is oriented normal to the atomizer and intersects the atomizer normal $\hat{\mathbf{z}}$ at a signed distance Ω_d along $\hat{\mathbf{z}}$, relative to the atomizer TCPF. We assume that the paint is emitted from a theoretical emission point \mathbf{e} located at a signed distance Ω_e along the atomizer normal relative to the TCPF. The distance from the emission point to the deposition model plane is given by $\Omega = \Omega_d - \Omega_e$. Given \mathbf{p} , Ω_d , and Ω_e , the paint emission point and deposition model plane are uniquely specified. The orientation of the deposition model plane about the z -axis $\hat{\mathbf{z}}$ of the atomizer is determined by the orientation of the atomizer assembly, and is independent of the direction of travel.

We choose to use a set of Gaussians as the basis for the planar deposition model because of the well-behaved analytic formula, widespread use in modeling natural phenomena, and expressive parameters. Experiments show a good match between Gaussian behavior and the actual deposition pattern on a planar surface; and hence, the planar paint deposition model uses two Gaussians: an offset 1-D Gaussian revolved about the z axis and a 2-D Gaussian centered at the origin of the deposition model plane. The revolved Gaussian term allows the model to capture a ring of heavier deposition observed in experiments.

Although the rotating bell is axially symmetric, the shaping air nozzles and pattern control ring are often not quite symmetric, and give rise to asymmetries found in actual deposition patterns [17]. An angle dependent scaling function is applied to the revolved Gaussian to generate these asymmetries in the model. Our model includes two types of asymmetry terms to capture these effects: a hemispheric weighting and a localized weighting.

The resulting planar deposition model, similar to the asymmetric volcano shown in Fig. 2, is given by

$$d(x, y) = K_1 \left(\frac{(1 - K_2)}{\gamma} f(x, y)g_1(x, y) + K_2 g_2(x, y) \right)$$

where $K_1 \in (0, \infty)$, which has units of thickness per second, scales the distribution to yield paint flux at a given point, and $K_2 \in [0, 1]$ weights the revolved Gaussian against the centered Gaussian. To account for asymmetry in the deposition pattern, the revolved offset Gaussian, $g_1: \mathbb{R}^2 \rightarrow \mathbb{R}$, is scaled by the function $f: \mathbb{R}^2 \rightarrow [0, 3]$. We define f to be

$$f(x, y) = \left(1 + K_3 \sin(\beta - \phi) + K_4 \exp \left(\frac{-(\cos(\beta - \rho) - 1)^2}{2\sigma_\rho^2} \right) \right)$$

where $\beta = \text{atan2}(y, x)$, $K_3 \in [0, 1]$ weights the hemispheric asymmetry scaling function oriented by the reference angle ϕ , and $K_4 \in [-1, 1]$ weights the asymmetry term localized by reference angle ρ with standard deviation σ_ρ . Note, the values of the parameters (K_3, K_4, ϕ , and ρ) are restricted such that $f(x, y) \in [0, 3]$.

The revolved offset Gaussian, g_1 , is symmetric so $g_1(x, y) = g_1(r)$ where $r = \sqrt{x^2 + y^2}$. We define g_1 to be

$$g_1(r) = \left(\exp \left(-\frac{(r - r_d)^2}{2\sigma_1^2} \right) + \exp \left(-\frac{(r + r_d)^2}{2\sigma_1^2} \right) \right) \quad (1)$$

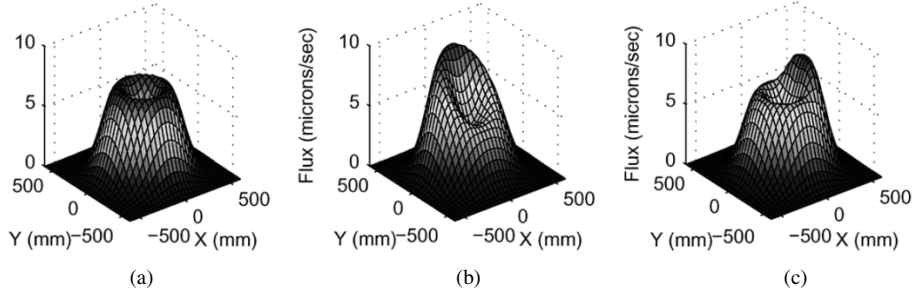


Fig. 4. These figures show the impact of the asymmetry terms K_3 and K_4 on the deposition pattern. For reference, $K_1 = 3.45$ (m/s), $K_2 = 0.25$, $r_d = 250$ mm, $\sigma_1 = 120$ mm, $\sigma_2 = 200$ mm, $\phi = 0$, $\rho = 0$, and $\sigma_\rho = 0.25$. (a) Symmetric pattern $K_3 = K_4 = 0$. (b) Hemispheric asymmetry $K_3 = 0.5$, $K_4 = 0$. (c) Localized asymmetry $K_3 = 0$, $K_4 = 0.5$.

where r_d is the offset radius and σ_1 is the standard deviation of the Gaussian. The scaling factor, γ , normalizes the deposition such that integral of $f \cdot g_1$ equals one, that is

$$\gamma = \int \int f(x, y) g_1(x, y) dy dx.$$

The centered Gaussian $g_2 : \mathbb{R}^2 \rightarrow \mathbb{R}$, is also symmetric and normalized, and is given by

$$g_2(x, y) = g_2(r) = \frac{1}{2\pi\sigma_2^2} \exp\left(-\frac{r^2}{2\sigma_2^2}\right)$$

where σ_2 is the standard deviation of the centered Gaussian. As the overall shape of the deposition pattern of an ESRB atomizer is approximately circular when the bell is oriented normal to a flat panel and the atomizer is stationary, our model uses a symmetric 2-D Gaussian.

Fig. 4 depicts some instances of this new deposition model. The images show the impact of changing the asymmetry terms in the model. Both asymmetry features can be rotated independently with respect to the deposition model plane.

2) *Surface Projection Model*: The planar model defined above predicts deposition on flat panels, with the atomizer oriented normal to the surface and located a fixed offset distance from the deposition surface. The next step is to predict paint deposition on arbitrarily shaped and oriented surfaces. We accomplish this using a direct geometric projection that preserves total paint volume, ignoring electrostatic and fluid dynamic effects of the paint spray [11], [12], [18]. We chose this projection model because typical car painting applications keep the bell atomizer at an approximately constant offset distance, and approximately normal orientation relative to the surface being painted.

The projection model, shown in Fig. 5 is developed by assuming that all of the paint emits from a point source called the emission point, e , which is constrained to lie along the bell-to-surface vector, \vec{z} . Note that this emission point is a theoretical emission point, not necessarily coincident with the actual center point of the bell atomizer. The planar deposition model is embedded orthogonal to the \vec{z} vector at a distance Ω from the emission point, with its x - y axes aligned with the x - y axes of the atomizer reference frame.

We define a set of parameterized curves, called projection curves. These curves model the set of paths a paint particle might take as it leaves the emission point. We derive a correspondence function that maps a point, s , on the target surface to

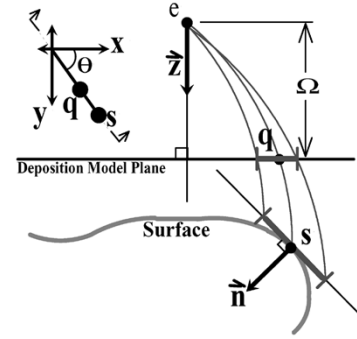


Fig. 5. Projection of deposition model onto an arbitrary surface. Note, the scaling effect of the patch projected from the deposition model plane to the surface approximation. Although the vectors are in reality three-dimensional, this simple figure conveys the basic results. (Note: The path location p is not shown).

a point, q , on the embedded deposition model plane. The point q is defined by the intersection of a projection curve, originating at e and passing through s , with the deposition model plane. The deposition flux impacting the surface point s is equivalent to the flux at q scaled by an area magnification factor, which ensures that the total paint volume is preserved.

For the projection curves, we define a family of polynomial curves, parameterized by $\xi \in [0, \infty)$, such that

$$\begin{pmatrix} x \\ y \\ z \end{pmatrix} (\xi) = \begin{pmatrix} \cos(\theta)\xi \\ \sin(\theta)\xi \\ C_f(x^2 + y^2)^{\frac{C_1}{2}} \end{pmatrix} = \begin{pmatrix} \cos(\theta)\xi \\ \sin(\theta)\xi \\ C_f \xi^{C_1} \end{pmatrix} \quad (2)$$

where θ determines the direction of the curve in the x - y plane, C_f scales the rate of increase of the z -coordinate, and C_1 determines the ‘‘curvature’’ of the curve. With a value of $C_1 = 1$, these curves are straight lines emanating from the emission point, e . As $C_1 \rightarrow \infty$, the curves bend sharply and asymptotically approach a line parallel to the atomizer normal, \vec{z} . The value of C_1 will be determined from data and then fixed; the values of C_f and θ are used to select a particular curve from a family of curves. The family of curves is well defined for any point on the deposition model plane, except for $(x, y) = (0, 0)$. In this special case, we allow the projection curve to be a straight line along the atomizer normal.

To derive the correspondence function, assume that we are given a target surface point $s = (x_s, y_s, z_s)$ with $(x_s, y_s) \neq (0, 0)$, and denote the corresponding deposition plane point $q = (x_q, y_q, z_q)$ with $z_q = \Omega$. Both points are specified in the atomizer coordinate system.

The parameters of the projection curve passing through an arbitrary point (x, y, z) are

$$\theta = \text{atan2}(y, x) \quad (3)$$

$$C_f = \frac{z}{(x^2 + y^2)^{\frac{C_1}{2}}}. \quad (4)$$

Note, for a single curve passing through the given points \mathbf{s} and \mathbf{q} , the curve parameters are the same. This allows us to derive the correspondence function $\varphi : \mathbb{R}^3 \rightarrow \mathbb{R}^3$ mapping target surface points to deposition plane points; that is

$$\begin{pmatrix} x_{\mathbf{q}} \\ y_{\mathbf{q}} \\ z_{\mathbf{q}} \end{pmatrix} = \varphi \begin{pmatrix} x_{\mathbf{s}} \\ y_{\mathbf{s}} \\ z_{\mathbf{s}} \end{pmatrix} = \begin{pmatrix} \left(\frac{\Omega}{z_{\mathbf{s}}}\right)^{\frac{1}{C_1}} x_{\mathbf{s}} \\ \left(\frac{\Omega}{z_{\mathbf{s}}}\right)^{\frac{1}{C_1}} y_{\mathbf{s}} \\ \Omega \end{pmatrix}.$$

To determine the area magnification factor, which measures the differential distortion between two surfaces, at a particular surface point $\mathbf{s} = (x_{\mathbf{s}}, y_{\mathbf{s}}, z_{\mathbf{s}})$, we first locally parameterize the surface at the point using the first-order approximation $\psi : \mathbb{R}^2 \rightarrow \mathbb{R}^3$. We define \mathbf{E}_1 and \mathbf{E}_2 to be orthogonal unit vectors that span the surface tangent plane at \mathbf{s} , such that the inward pointing surface normal is $\vec{\mathbf{n}} = \mathbf{E}_1 \times \mathbf{E}_2$. Thus, in the neighborhood of \mathbf{s} the surface is approximated by

$$\psi(u, v) = \mathbf{s} + u\mathbf{E}_1 + v\mathbf{E}_2$$

where u and v are parameters of the local mapping.

Next, we use the correspondence function to map this local neighborhood of the target surface onto the deposition plane. The combined mapping is

$$\begin{aligned} & (\varphi \circ \psi)(u, v) \\ &= \begin{pmatrix} (uE_{11} + vE_{21} + x_{\mathbf{s}}) \left(\frac{\Omega}{uE_{13} + vE_{23} + z_{\mathbf{s}}}\right)^{\frac{1}{C_1}} \\ (uE_{12} + vE_{22} + y_{\mathbf{s}}) \left(\frac{\Omega}{uE_{13} + vE_{23} + z_{\mathbf{s}}}\right)^{\frac{1}{C_1}} \\ \Omega \end{pmatrix} \end{aligned}$$

where E_{ij} denotes the j th component of \mathbf{E}_i .

The first fundamental form of this combined mapping gives the relationship between areas in the u, v space and areas on the deposition plane [19]. Evaluating the first fundamental form at $(u = 0, v = 0)$ gives the area magnification factor

$$AM(\mathbf{s}, \mathbf{p}) = \sqrt{\frac{\left(\frac{\Omega}{z_{\mathbf{s}}}\right)^{\frac{4}{C_1}} ((\mathbf{E}_1 \times \mathbf{E}_2) \cdot (x_{\mathbf{s}}, y_{\mathbf{s}}, C_1 z_{\mathbf{s}}))^2}{C_1^2 z_{\mathbf{s}}^2}}.$$

A more explicit derivation of the area magnification factor for a linear projection is given in [20].

Substituting the surface normal definition and simplifying, we obtain

$$AM(\mathbf{s}, \mathbf{p}) = \begin{cases} \left(\frac{\Omega}{z_{\mathbf{s}}}\right)^{\frac{2}{C_1}} \begin{pmatrix} \frac{x_{\mathbf{s}}}{C_1 z_{\mathbf{s}}} \\ \frac{y_{\mathbf{s}}}{C_1 z_{\mathbf{s}}} \\ 1 \end{pmatrix} \cdot \vec{\mathbf{n}} & \text{if } \begin{pmatrix} \frac{x_{\mathbf{s}}}{C_1 z_{\mathbf{s}}} \\ \frac{y_{\mathbf{s}}}{C_1 z_{\mathbf{s}}} \\ 1 \end{pmatrix} \cdot \vec{\mathbf{n}} > 0 \\ 0 & \text{otherwise.} \end{cases}$$

The area magnification goes to zero as the projection curve becomes tangent to the surface. If the dot product above is negative, it indicates that the projection curve is intersecting the target surface from the incorrect side and thus the surface should not receive any paint deposition.

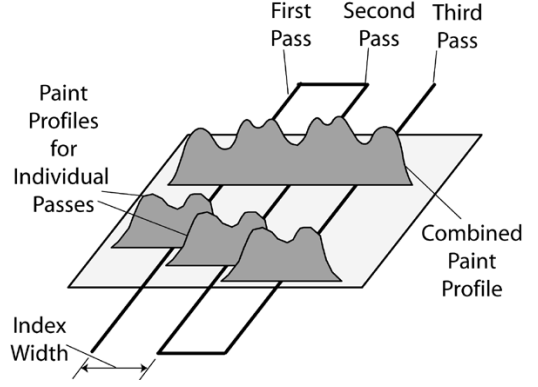


Fig. 6. Painting a flat panel with three passes.

3) *Speed Flux Scaling*: The final component of our paint deposition model on an arbitrary surface is a scaling due to the speed of the TCPF. Our early experiments indicated that paint deposition flux may vary with speed. Ford personnel speculate that some paint droplets may actually bounce off of dry surfaces [17]. As the droplets bounce less on wet surfaces, this causes an increase in transfer efficiency as paint builds up on the surface. Thus, we theorize that faster atomizer motion allows less time for paint to build up, thereby decreasing the relative transfer efficiency.

Our composite model includes a simple model for scaling the flux due to changes in atomizer speed of the form

$$V_s(\dot{\mathbf{p}}) = \left(1 + k_1 \left(\frac{1}{\|\dot{\mathbf{p}}\|_t} - \frac{1}{v_{\text{nom}}}\right)\right)$$

where k_1 is a parameter to be fit to the data, $\|\dot{\mathbf{p}}\|_t$ is the translational speed of the atomizer TCPF, and v_{nom} is the nominal translation speed of the TCPF.

B. 1D Collapse Model

In order to control the amount of variation in the coating thickness, a trajectory planner must know the relationship between the deposition pattern of the atomizer, the trajectory followed, and the resulting deposition on the surface being painted. Typically, the deposition pattern is narrower than the width of the surface being painted, requiring multiple passes to completely cover the surface as shown in Fig. 6.

As the bell moves relative to the surface, as shown in Fig. 2, the 2-D deposition pattern moves over the surface and paint is accumulated at each point on the surface. We use the 1-D collapse to allow us to analytically consider the thickness variation effects of varying the *index distance* (distance between adjacent passes).

The 1-D collapse models the accumulated film thickness profile as a function of the distance perpendicular to the direction of travel, assuming that the deposition pattern does not vary with time or position along the surface. This restricts our definition of the 1-D collapse to planes, extruded surfaces, or half cylinders. For general extruded surfaces, the trajectories are defined along the axis of extrusion; for the special case of half cylinders, the trajectories are defined along the cylinder axis or

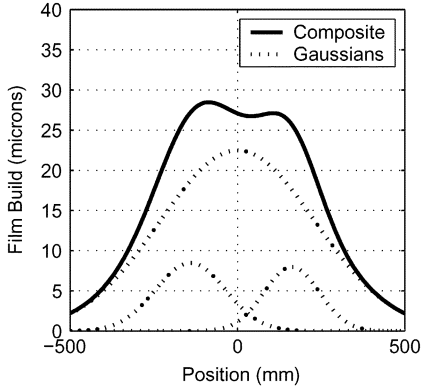


Fig. 7. Asymmetric 1-D collapse model with component Gaussians shown.

geodesics around the cylinder [20]. Unfortunately, the structure of the analytic 2-D deposition model renders the calculation of a closed form integral expression for the total deposition intractable. Therefore, we directly define a 1-D collapse model as

$$c(x) = \frac{1}{3\sqrt{2\pi}} \sum_{i=1}^3 \frac{\kappa_i}{\sigma_i} \exp\left(-\frac{(x-r_i)^2}{2\sigma_i^2}\right) \quad (5)$$

where x is measured in the surface, orthogonal to the direction of travel. The three exponential terms that constitute this model are each normalized Gaussians, with r_i representing the center locations and σ_i the standard deviations. The first two Gaussians are offset from the centerline, such that $r_1 > 0$ and $r_2 < 0$, to capture asymmetries in the deposition pattern; the third Gaussian is centered with $r_3 = 0$. The gains κ_i are used to specify the paint flux for each Gaussian. Fig. 7 shows the component Gaussians and the associated composite film build for a particular set of parameter values for (5). Note this model assumes a particular atomizer speed and orientation. It will, in general, have different parameter values for different speeds and orientations due to the asymmetry and speed dependence of the 2-D deposition pattern.

To develop an understanding of how the deposition pattern and index distance interact to determine thickness variation, we ignore boundary effects and limit our discussion to an infinite planar surface painted by an infinite number of passes, with the atomizer at a consistent orientation relative to the plane and moving at a constant speed. The total thickness at x is given by

$$T(x, \Delta x) = \sum_{i=-\infty}^{\infty} c(x + i\Delta x) \quad (6)$$

where Δx is the index distance, and $c(\cdot)$ is the 1-D collapse model for the given speed and orientation relative to the direction of travel. Looking at the thickness measurements as we vary x , the measurement pattern repeats itself with a period equal to the index distance. The normalized deviation over one index is given by

$$\sigma(\Delta x) = \left(\frac{1}{\Delta x} \int_{-\frac{\Delta x}{2}}^{\frac{\Delta x}{2}} \left(\frac{T(x, \Delta x)}{\bar{T}(\Delta x)} - 1 \right)^2 dx \right)^{1/2} \quad (7)$$

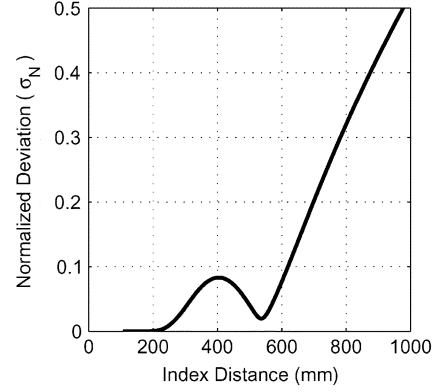


Fig. 8. Normalized deviation versus index distance for a typical 1-D collapse.

where \bar{T} is the average thickness over the interval. We use numerical integration to evaluate (7) due to the complexity of the equations in the numerator.

A typical deviation versus index distance curve for a particular set of 1-D collapse parameter values is shown in Fig. 8. As expected, large indexes yield high deviation. If the model was only a single center Gaussian, the deviation versus index distance curve would be a monotonically increasing function. However, in cases where there are significant offset Gaussian terms, there is a local minimum in deviation versus index distance curve. The existence of this “sweet spot” may allow the use of larger index distances to generate paint coverage with acceptable variation, while reducing total cycle time. The deviation tends to be sensitive to changes in index distance at the sweet spot, so for tight tolerances, keeping index distances smaller than the sweet spot local minimum may be advisable.

Using both the 2-D deposition model and 1-D collapse model allows us to perform parametric studies of the variation in paint thickness. The 2-D deposition model is used to predict paint deposition on a surface as a function of speed, orientation, and various parameters. The 1-D collapse model, whose parameters can be fit to the deposition profile predicted by the 2-D model or determined experimentally, allows the direct computation of the resulting variation. This allows us to analyze the effects of changes to any of the 2-D deposition model’s variables.

IV. DEPOSITION MODEL FITTING AND VALIDATION

In order to determine the proper model parameters and validate our models, we conducted a series of experiments at the ABB Process Automation facility in Auburn Hills, Michigan. The experiments used an ABB S3 robot outfitted with an ABB 50 mm Micro-Micro Bell atomizer to apply a solvent based automotive paint to phosphate coated test panels and primed automotive surfaces. The operating conditions of the application process were 80–90-kV electrostatic voltage, 300-cc/min paint flow, 300-nl/min shaping air flow, and a bell speed of 30000 RPM. The nominal speed of the atomizer was 200 mm/s, although the speed was varied in some of the experiments, as specified below.

The total film thickness profile of the oven cured test panels was measured with an Elcometer 355 coating thickness measuring device. Five measurements were taken for each data

point, with the low and high discarded and the average of the remaining three recorded. To obtain data for the paint film build on the primed or phosphate coated metal, the average primer/phosphate thickness was subtracted from the average total film thickness data to give the paint thickness value.

In this section, we describe the experiments used to fit and validate each of the 2-D deposition model components—planar deposition model, projection model, and speed scaling model—and then describe a series of experiments on an actual automotive surface using the fit model. The 1-D collapse model can be fit to the same data; however, this section will only present the results for the 2-D model, which is used for predicting paint deposition given a surface and a specified trajectory.

A. Planar Deposition Model

The planar deposition model has ten total parameters ($K_1, K_2, r, \sigma_1, \sigma_2, K_3, K_4, \phi, \rho, \sigma_\rho$). The first five of these parameters are “symmetric” parameters with respect to an emission axis as described in Section III. The second five parameters are “asymmetric” parameters used to model asymmetries in the deposition pattern.

An obvious method of fitting these parameters to the data would use a deposition pattern generated by a stationary atomizer. Unfortunately, these patterns tend to be unreliable because of the differing thickness values across the deposition pattern. The thickness ranges from disconnected droplets of paint spatter on the border, to thick rings of paint deposition. Early tests found that aggregate results, obtained by using thickness profiles of deposition from constant velocity trajectories, resulted in more reliable data. As the edges of the deposition pattern tend to have less paint, we chose to use multiple parallel passes to build up a consistent thickness for measuring the deposition.

Our experiments use three passes over a flat panel, as shown in Fig. 6, to determine the values of these parameters. In each experiment, the flat panels were mounted on a vertical surface during paint application. The paint atomizer applied paint in three passes spaced at a constant index distance. The atomizer was located at an offset of 254 mm from the panels and oriented with its emission axis normal to the surface. As the TCPFs are located on the surface, the physical arrangement parameters are $\Omega_d = 0$ and $\Omega_e = -254$ mm. The atomizer moved on the three-pass path at a constant nominal speed of 200 mm/s. To guarantee a reliable paint thickness for measurement, each pass was covered twice by the paint atomizer. This double coverage has the effect of averaging the deposition pattern. The paint deposition thickness profile was measured orthogonal to the travel direction, as shown in the Fig. 2.

A total of seven tests were conducted. To capture the asymmetries, two experiments with the same index distance were conducted for 475, 525, and 575-mm index distances. The first experiment used vertical painting passes over a vertical surface, while the second used horizontal passes over a vertical surface with the same atomizer orientation as the first. A vertical test with 300-mm spacing was also conducted.

For our model fitting, we chose to use the test with an index distance of 525 mm. This distance allowed sufficient overlap to

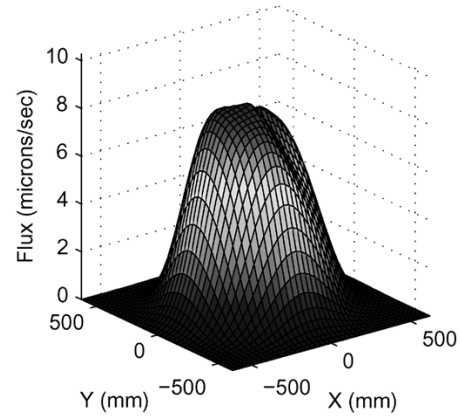


Fig. 9. Resulting 2-D Model that was fit to experimental data.

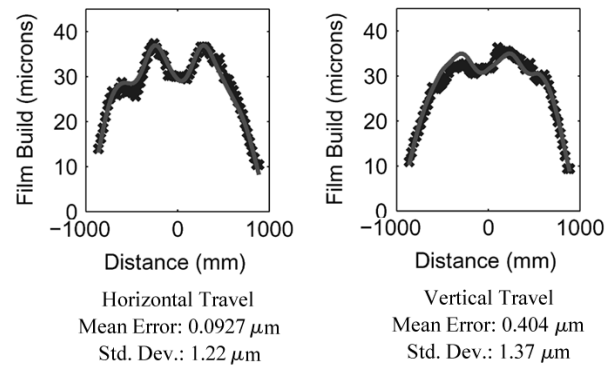


Fig. 10. Data versus fit for 3-pass test with 525 mm index distance.

build up measurable thickness on the boundary, while retaining a distinctive thickness profile. The fitting procedure used numerical optimization tools, beginning with an initial guess for the model parameter values. Given a particular set of parameter values for the planar deposition model, the model’s prediction of the data from a single three-pass test was produced in two steps. First, the planar deposition model was numerically integrated in the direction of travel to produce a 1-D thickness profile from the 2-D model. This thickness profile was then offset by the index distance to simulate each pass. The resultant predictions were summed to create the full thickness profile predicted for three passes of the deposition pattern. This yielded the model’s prediction of the measured data for a given travel direction. This process was performed for both horizontal and vertical travel directions.

The predicted thickness profile values, obtained by integrating the simulated 2-D deposition pattern, were compared to the observed data in a point-wise fashion for the horizontal and vertical travel directions. Given the deposition data set and a set of initial parameter values, the parameters were numerically optimized using the total sum of squared errors for both travel directions as the cost function. Penalties for approaching constraints, such as the radius and deviation parameters being positive, were added to the cost.

The resulting parameters produced by this method are $K_1 = 3.44$ m/s, $K_2 = 0.278$, $r = 258$ mm, $\sigma_1 = 121$ mm, $\sigma_2 = 144$ mm, $K_3 = 0.362$, $K_4 = -0.974$, $\phi = 1.15$ rad, $2\rho = 0.306$ rad, and $\sigma_\rho = 1.13$ rad. Fig. 9 shows the planar deposition

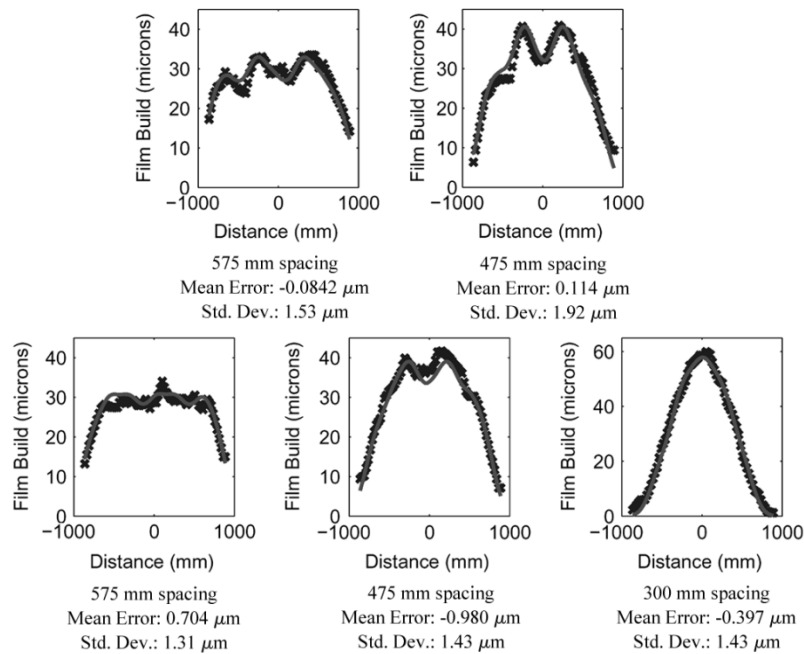


Fig. 11. Data (x) versus prediction (—) for 3-pass planar model validation tests. Upper row = horizontal passes, lower row = vertical passes.

model surface for these parameters. Fig. 10 shows the comparison between the model prediction and the experimental data from the 525-mm index tests.

The planar deposition model was validated by comparing the predicted paint thickness with experimental results from the remaining three-pass flat panel experiments at 300-, 475-, and 575-mm spacing. Using the 2-D deposition model fitted to the 525-mm index three-pass test data as described above, the depositions generated by the trajectories of the validation tests were predicted. The resultant comparison between experiment and prediction are shown in Fig. 11.

The model gives a good prediction of both average film build and the structure of the variation for these flat panel tests. Most importantly, the model captured both the asymmetries and the structural variation dependence on index distance.

B. Surface Projection Model

The projection model has a single parameter, C_1 , which determines the “curvature” of the projection curves. In order to determine the value of this parameter, we performed two types of tests: cylinder tests and oblique angle tests.

In the cylinder tests, a cylindrical surface of constant radius was placed with its axis pointing vertically. A single pass of the atomizer parallel to the axis of the cylinder was used to apply paint. To guarantee a reliable paint thickness for measurement, each pass was covered twice by the paint atomizer. The atomizer was maintained at a constant offset of 254 mm and oriented normal to the cylinder surface. Data were taken from a 1-D curve wrapping around the cylinder orthogonal to the atomizer travel direction. The cylinder tests were performed on four different radii cylinders: 250, 500, 750, and 1000 mm.

In the oblique angle tests, a flat panel was mounted vertically and painted with a single horizontal pass. Again, the single pass

was covered twice by the paint atomizer to generate an adequate film build. The atomizer was located at a constant offset of 254 mm away from the flat panel and oriented with its emission axis tilted with respect to the normal of the flat panel. The atomizer was angled to point upward with respect to a horizontal plane, so that there was a component of tilt only in the vertical direction. Data were taken from a 1-D profile orthogonal to the travel direction. The oblique angle tests were performed at two orientations; the atomizer was tilted 10° and 20° with respect to the flat panel normal.

In order to predict deposition on each of these surfaces, the planar 2-D deposition model, whose parameters were fit in Section IV.A, was projected onto the surface using the surface projection model with the current value for the C_1 parameter. This projected pattern was numerically integrated in the travel direction to produce the prediction of the 1-D profile, which was compared to the experimental data to obtain the error. We chose to use the 500 and 750 mm radius cylinders and the 20° oblique tests for parameter estimation. The fitting procedure discarded data points with thickness measurements less than $8 \mu\text{m}$, to avoid measurement problems due to droplet spatter. The sum of squared error between the remaining data points and model prediction for all three tests was used as the cost function for our optimization.

We used a standard numeric optimization technique to minimize this error as a function of C_1 . A collection of optimized values was obtained by using initial values of $C_1 = 1$, a linear projection, and $C_1 = 5, 10$, and 100. A value of $C_1 = 2.52$ was selected from the optimized collection.

The resultant prediction of paint deposition on each of the training data sets is shown in Fig. 12. As shown, the model fits the data for the cylinders, but does not do a good job capturing the distortion due to the oblique tests. This is most likely due to unmodeled electrostatic effects.

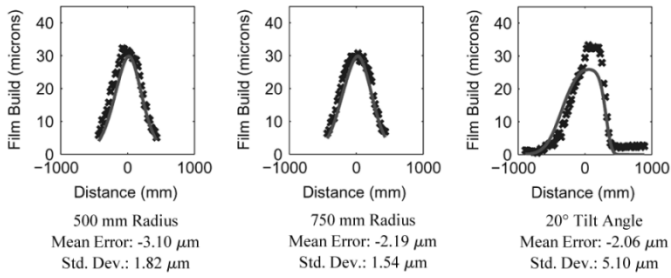


Fig. 12. Data versus fit for surface projection model training tests using cylinders and a tilted plane.

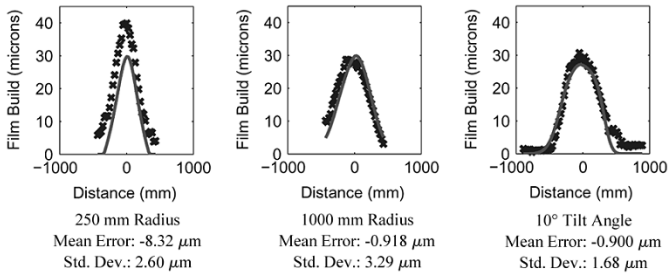


Fig. 13. Data (x) versus prediction (—) for surface validation tests using cylinders and a tilted plane.

The 250- and 1000-mm cylinder tests and 10° oblique angle tests were chosen as the validation tests for the projection model. The results of the model’s prediction of these data sets is shown in Fig. 13. Here, the model fails to capture the distortion on the small radius cylinder; again, most likely due to electrostatic effects. In fact, the model under predicts the total deposition significantly. It is theorized that, while our model predicts paint loss due to over-spray, the electrostatic field acts to draw paint back toward the surface. This boundary effect is not evident on the flat panel tests because the panels are mounted to a larger grounded flat metal surface.

The prediction for the 1000-mm radius cylinder appears to be slightly shifted. This is most likely due to an error in the setup of the test cylinder, which was manufactured from two pieces of steel welded together. The deposition thickness prediction for this larger radius cylinder is more accurate than that of the smaller 250-mm radius cylinder. Likewise, the match for the slightly oblique flat panel is more accurate than for the more oblique 20° panel or the smaller radii cylinders. Again, these effects can be explained by the lack of an explicit electrostatic field calculation in our model. The electrostatic effects begin to dominate as curvature of the surface or the relative angle between the atomizer axis and surface normal increases. In spite of this deficiency, the model does appear to capture the basic structure of the distortion.

C. Speed Scaling Model

To determine the value of the speed scaling parameter, k_1 , a series of flat panel experiments were performed, where a single pass of the atomizer was used to paint the panels. Once again, the pass was covered twice to guarantee a reliable paint thickness for measurement.

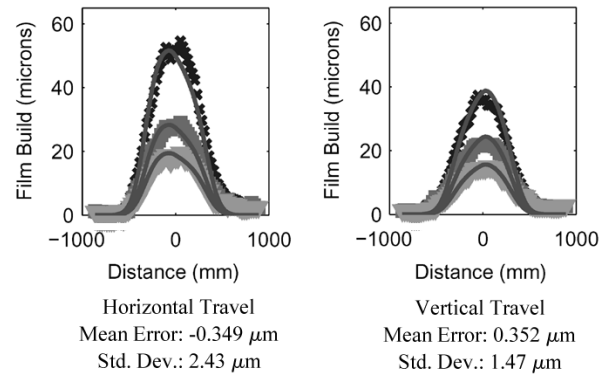


Fig. 14. Data versus prediction (—) for speed scaling training tests. (Top to bottom, the curves are for 150, 250, 400 mm/s speeds respectively).

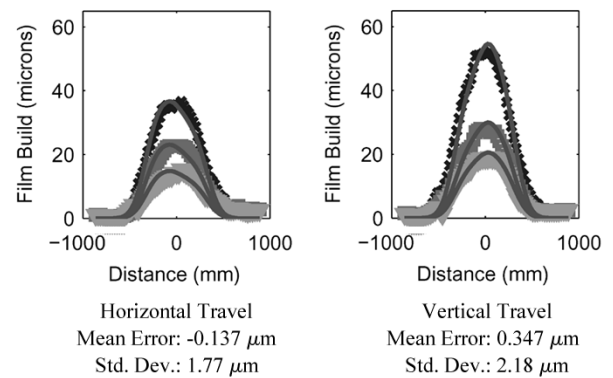


Fig. 15. Data versus prediction (—) for speed scaling validation tests. (Top to bottom, the curves are for 100-, 200-, 300-mm/s speeds, respectively).

In each of these experiments, the flat panels were mounted on a vertical surface during paint application. The atomizer was located at an offset of 254 mm from the panels and oriented with its emission axis normal to the surface. The panels were painted at six different speeds 100, 150, 200, 250, 300, and 400 mm/s. The tests were performed for both horizontal and vertical passes of the atomizer. In total, twelve tests were performed. The data taken from each test was a 1-D deposition profile orthogonal to the travel direction.

The parameter fitting algorithm used data from the 100-, 200-, and 300-mm/s horizontal passes and the 150-, 250-, and 400-mm/s vertical passes. The resultant paint deposition obtained by numerically integrating the 2-D paint deposition pattern, whose parameters were determined in Section IV.A, was compared in a point-wise fashion to the observed paint deposition data. Once again, our fitting procedure discarded data points with thickness measurements less than 8 μm. The total error between the observed deposition and predicted deposition was used to determine the cost. The k_1 parameter was selected by minimizing the total error cost. The comparison between the model prediction and the experimental data is shown in Fig. 14, where $k_1 = -11.4$.

The data from the remaining speed tests—that is, the 150-, 250-, and 400-mm/s horizontal passes and the 100-, 200-, and 300-mm/s vertical passes—were used to validate the parameter fit. The results of these tests are shown in Fig. 15. As can be

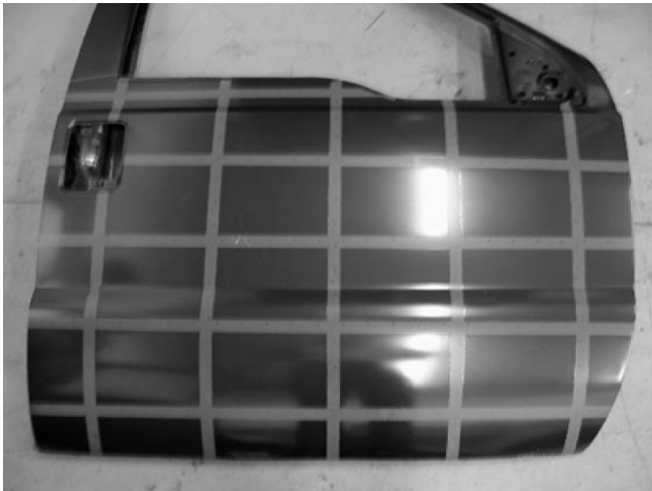


Fig. 16. A painted excursion door. The baseline data strips run both vertically and horizontally.

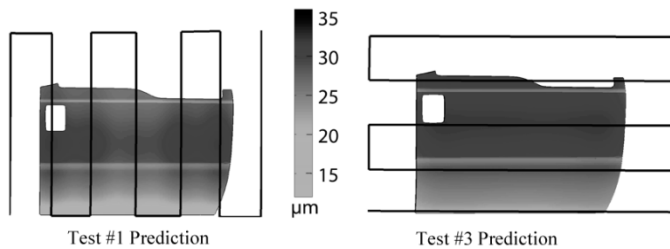


Fig. 17. Predicted paint deposition on door. Paths are shown as solid dark lines over the door.

seen in the graphs, the model does accurately capture the slight dependency of deposition flux on speed.

D. Complete Deposition Model

To validate the performance of the full model consisting of the planar deposition model, speed scaling and surface projection models, the Ford Excursion passenger side front door was chosen as a target surface. Fig. 16 shows one of the doors used in our experiments. The door has a line of concave curvature near the middle, with a pronounced convex curvature on the bottom third of the door.

A series of four paint deposition tests were conducted on primer coated Ford Excursion doors. For each test, the door was mounted to be approximately vertical. The atomizer emission axis was maintained normal to the surface. In two of the tests, the door was painted with horizontal atomizer passes, and the other two tests were performed with vertical passes. The paths on two of the doors are shown in Fig. 17.

These door tests were also intended to validate our early trajectory planning methods, so both the speed along the pass and index distance between the passes varied in some tests. A summary of the salient characteristics of each test is shown in Table I. In this paper, our focus is on how well the predicted paint deposition matches the actual deposition, and not on the relative performance of the different trajectories.

Before painting, vertical and horizontal 25.4-mm wide tape strips were placed on the door to prevent paint application, and

TABLE I
SUMMARY OF DOOR EXPERIMENTAL SETUP

Test	min/nominal/max Speed	min/max Index	Travel Direction
Test 1	100/200/400 mm/sec	160/400 mm	Vertical
Test 2	200/200/200 mm/sec	160/400 mm	Vertical
Test 3	100/200/400 mm/sec	250/310 mm	Horizontal
Test 4	100/200/400 mm/sec	400/400 mm	Horizontal

TABLE II
SUMMARY OF DOOR EXPERIMENT RESULTS

Test	Mean Error	Standard Deviation
Test1	-4.38 μm	4.20 μm
Test2	-6.48 μm	4.41 μm
Test3	-3.04 μm	3.98 μm
Test4	-1.47 μm	3.52 μm

thus provide a location for measuring the primer thickness. The spacing of the strips, shown in Fig. 16, was 184 mm for the horizontal strips and 254 mm for the vertical strips. After painting, the tape strips were removed and the paint oven cured. For each door, a 5 row \times 5 column grid of data points covering the door was taken. Within each unpainted strip, baseline primer measurements were taken at 50.8-mm spacing. Baseline primer data were important for the Ford Excursion door tests, since primer thickness was known to vary significantly across the surface. Paint deposition data were taken at a point offset from each baseline data point; 25.4 mm to the left for vertical strips and 25.4 mm below for horizontal strips. The paint deposition at the data point was calculated by the total film build measured at the data point minus the film build at the baseline data point.

To predict paint deposition on the door, the robot trajectories were simulated on a CAD model of the Ford Excursion door. The actual robot path locations, which specify the robot trajectories, were interpolated to give a fine resolution set of simulation points, which approximate the robot trajectory. The simulation points were approximately 8 mm apart. The simulation time spent at each point was calculated based on the average speed, also interpolated between actual path locations, and the distance to neighboring simulation points. The contribution of paint at a particular simulation point on the triangulated surface from a given point was calculated as the deposition flux given by the 2-D deposition model multiplied by the time spent at the given point. The total paint deposition for a given point on the triangulated surface was the sum of the predicted paint deposition at that point for all of the simulation points. A summary of the results for all of the data points on each door is shown in Table II. Fig. 18 shows selected thickness profiles for the first test; the other tests have similar profiles.

Overall, although the model captured the basic structure of the paint deposition, the model under-predicted the paint deposition on these automotive surfaces. It is theorized that when the surface curves away from the atomizer, as shown in Fig. 5, the electrostatic effects become more prominent, which partially invalidates the geometric projection model described in Section III. This effect is especially prevalent near the edges of the door. Our model predicts that paint droplets would be lost, when the electrostatic effects could actually bend the trajectories back to the edges of the door.

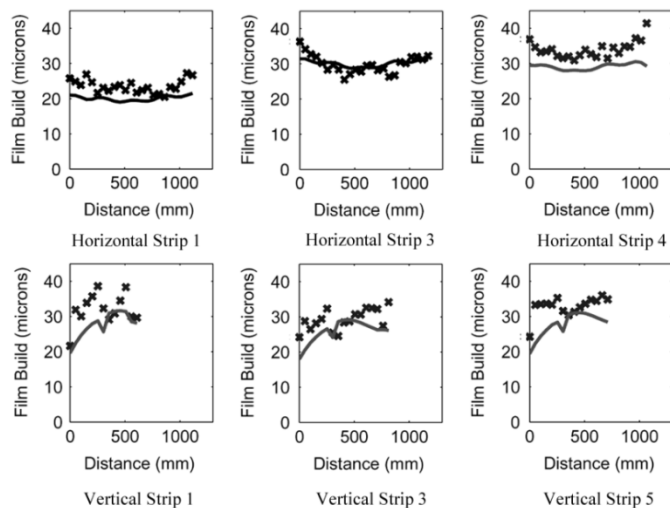


Fig. 18. Data (x) versus prediction (—) for door test #1.

V. CONCLUSION

The results of our experimental study lead us to conclude that our models capture the relevant structure of the planar deposition pattern, and the dependence of the thickness variation on that structure. It is also apparent that the interaction of the paint droplets emitted from the atomizer and the surface curvature has a significant impact on the actual deposition pattern on curved surfaces. These preliminary conclusions also indicate the need for additional tests regarding the dependence of the deposition pattern and transfer efficiency on the speed of the atomizer as it moves relative to the surface.

The models we have developed accurately predict deposition on planar surfaces, where the atomizer is oriented normal to the surface. Although the experimental results from deposition on the curved door surface point to shortcomings with the simple geometric projection developed in Section III, the experiments do confirm the interaction of surface curvature with the planar deposition pattern.

Despite the shortcomings of our 2-D deposition model, the models are useful for research. By using an analytic model, we are able to develop our understanding of the interaction between the surface, the deposition pattern, and the atomizer path. This enables our exploration of trajectory planning techniques that influence overall quality measures such as thickness variation, cycle time, and efficiency. We will continue to use these analytic models during the development phase of our planning tools. Given that our planning tools rely only on the structure of the deposition on the surface, and not on the underlying model, the need for more computationally expensive models or experimental data is delayed until the implementation stage.

ACKNOWLEDGMENT

The authors gratefully acknowledge the input and support provided by Dr. J. Braslaw and Mr. J. Petty, their collaborators at the Ford Motor Company. They also sincerely thank Mr. T. Wang from the Ford Motor Company and Mr. G. Marsh, Mr.

N. Gauci, Mr. M. Bichel, Mr. R. Mata, and Mr. D. Smith from ABB for the help carrying out experiments at the ABB facility in Auburn Hills, MI, USA.

REFERENCES

- [1] P. N. Atkar, D. C. Conner, A. Greenfield, H. Choset, and A. A. Rizzi, "Uniform coverage of simple surfaces embedded in \mathbb{R}^3 for auto body painting," in *Proc. Workshop on Algorithmic Foundations of Robotics*, Utrecht/Zeist, The Netherlands, Jul. 2004, pp. 383–398.
- [2] P. N. Atkar, H. Choset, and A. A. Rizzi, "Toward optimal coverage of 2-dimensional surfaces embedded in \mathbb{R}^3 : Choice of start curve," in *Proc. IEEE/RSJ Int. Conf. Intelligent Robots and Systems*, vol. 3, Las Vegas, NV, 2003, pp. 3581–87.
- [3] E. U. Acar, H. Choset, A. A. Rizzi, P. N. Atkar, and D. Hull, "Exact cellular decompositions in terms of critical points of morse functions for sensor-based coverage tasks," *Int. J. Robot. Res.*, vol. 4, pp. 331–344, Apr. 2002.
- [4] E. U. Acar and H. Choset, "Sensor-based coverage of unknown environments: Incremental construction of exact cellular decompositions in terms of critical points of morse functions," *Int. J. Robot. Res.*, vol. 21, no. 4, pp. 345–366, Apr. 2002.
- [5] P. N. Atkar, H. Choset, A. A. Rizzi, and E. U. Acar, "Exact cellular decomposition of closed orientable surfaces embedded in \mathbb{R}^3 ," in *Proc. IEEE Int. Conf. Robotics and Automation*, vol. 1, Seoul, Korea, May 2001, pp. 699–704.
- [6] S.-H. Suh, I.-K. Woo, and S.-K. Noh, "Development of an automated trajectory planning system (ATPS) for spray painting robots," in *Proc. IEEE Int. Conf. Robotics and Automation*, Sacramento, CA, Apr. 1991, pp. 1948–1955.
- [7] N. Asakawa and Y. Takeuchi, "Teachless spray-painting of sculptured surface by an industrial robot," in *Proc. IEEE Int. Conf. Robotics and Automation*, vol. 3, Albuquerque, NM, Apr. 1997, pp. 1875–79.
- [8] W. Sheng, N. Xi, M. Song, Y. Chen, and P. MacNeille, "Automated CAD-guided robot path planning for spray painting of compound surfaces," in *Proc. IEEE/RSJ Int. Conf. Intelligent Robots and Systems*, 2000, pp. 1918–1923.
- [9] E. Freund, D. Rokossa, and J. R. mann, "Process-oriented approach to an efficient off-line programming of industrial robots," in *Proc. IEEE Industrial Electronics Society Conf. (IECON)*, vol. 1, 1998, pp. 208–213.
- [10] R. Ramabhadran and J. K. Antonio, "Fast solution techniques for a class of optimal trajectory planning problems with applications to automated spray coating," *IEEE Trans. Robot. Autom.*, vol. 13, no. 4, pp. 519–530, Aug. 1997.
- [11] M. A. Sahir and T. Balkan, "Process modeling, simulation, and paint thickness measurement for robotic spray painting," *J. Robot. Syst.*, vol. 17, no. 9, pp. 479–494, 2000.
- [12] P. Hertling, L. Hög, R. Larsen, J. W. Perram, and H. G. Petersen, "Task curve planning for painting robots—Part I: Process modeling and calibration," *IEEE Trans. Robot. Autom.*, vol. 12, no. 2, pp. 324–330, Apr. 1996.
- [13] Smartpainter—A Fully Automated Robot Painting System (2003, May). [Online]. Available: <http://www.mip.sdu.dk/research/Smartpainter/index.html>
- [14] K. R. J. Ellwood and J. Braslaw, "A finite-element model for an electrostatic bell sprayer," *J. Electrostat.*, vol. 45, no. 1, pp. 1–23, 1998.
- [15] A. A. Elmoursi, "Electrical characterization of bell-type electrostatic painting systems," *IEEE Trans. Ind. Appl.*, vol. 28, no. 5, pp. 1174–1180, Oct. 1992.
- [16] H. Huang and M.-C. Lai, "Simulation of spray transport from rotary cup atomizer using KIVA-3V," in *Proc. ICLASS'00*, Pasadena, CA, Jul. 2000, pp. 1435–1437.
- [17] J. Braslaw, private communication, 2001.
- [18] H. Chen, W. Sheng, N. Xi, M. Song, and Y. Chen, "Automated robot trajectory planning for spray painting of free-form surfaces in automotive manufacturing," in *Proc. IEEE Int. Conf. on Robotics and Automation*, vol. 1, Washington, DC, May 2002, pp. 450–55.
- [19] J. Thorpe, *Elementary Topics in Differential Geometry*. New York: Springer-Verlag, 1979.
- [20] D. C. Conner, P. N. Atkar, A. A. Rizzi, and H. Choset, "Deposition Modeling for paint application on surfaces embedded in \mathbb{R}^3 for use in automated trajectory planning," Robotics Institute, Carnegie Mellon, Pittsburgh, PA, Tech. Rep. CMU-RI-TR-02-08, Jun. 2002.



David C. Conner (S'00) received the B.S. and M.S. degrees in mechanical engineering from Virginia Tech., Blacksburg, in 1991 and 2000, respectively, and the M.S. degree in robotics from Carnegie Mellon University, Pittsburgh, PA, in 2004. He is currently working toward the Ph.D. degree in robotics at the same university.

Prior to entering graduate school, he served as Lead Engineer for TRAX Corporation, Lynchburg, VA, where he developed industrial process simulations. His research interests include applications of differential geometry, hybrid systems, and control theory to mobile robot navigation and control.



Aaron Greenfield (S'05) received the B.S. degree in computer science from Stanford University, Stanford, CA, in 2001, and is currently working toward the Ph.D. degree at the Robotics Institute, Carnegie Mellon University, Pittsburgh, PA.

His research interests include path planning for spray painting applications, climbing techniques for hyperredundant robotics, and the broader area of automatic manipulation.



Prasad N. Atkar (S'04) received the B.E. degree in mechanical engineering from Visvesvaraya Regional College of Engineering (now VNIT), Nagpur, India, in 1998, and the M.S. and Ph.D. degrees in mechanical engineering from Carnegie Mellon University, Pittsburgh, PA, in 2000 and 2005, respectively.

His research interests include surface coverage, robot motion planning, applied differential, and computational geometry.



Alfred A. Rizzi (M'89) received the B.Sc. degree from the Massachusetts Institute of Technology, Cambridge, MA, in 1986, and the M.S. and Ph.D. degrees from Yale University, Cambridge, MA, in 1990 and 1994 respectively, all in electrical engineering.

Prior to entering graduate school, he served as a Design Engineer with the Northrop Corporation, Anaheim, CA. He is currently an Associate Research Professor in the Robotics Institute, Carnegie Mellon University, Pittsburgh, PA. His research focus includes a combination of topics related to dynamically capable robotic systems, as well as industrial and commercial application of such systems.

Dr. Rizzi is a member of the editorial board for the *International Journal of Robotics Research*.



Howie Choset (M'94) received the Ph.D. degree in mechanical engineering from the California Institute of Technology, Pasadena, CA, in 1996.

He is currently an Associate Professor in Robotics at the Robotics Institute, Carnegie Mellon University, Pittsburgh, PA, where he conducts research in motion planning and design of serpentine mechanisms, coverage path planning for de-mining and painting, mobile robot sensor based exploration of unknown spaces, and education with robotics.

Dr. Choset was awarded the National Science Foundation Career Award to develop motion planning strategies for arbitrarily shaped objects in 1997, and support from the Office of Naval Research under the Young Investigator Program to develop strategies to search for land and sea mines, since 1999. The MIT Technology Review elected him as one of its top 100 innovators in the world under 35.